Progress In Electromagnetics Research Letters, Vol. 51, 53–59, 2015

Omnidirectional Low-Profile Multiband Antenna for Vehicular Telecommunication

Woncheol Lee[1], Yang-Ki Hong[1, *], Jaejin Lee[1], Jihoon Park[1], and Won-Mo Seong[2]

Abstract—An omnidirectional low-profile multiband antenna is designed and fabricated for vehicular telecommunication applications. The fabricated antenna with a radiator patch size of $0.26\lambda_L \times 0.3\lambda_L$ has a low-profile of $0.022\lambda_L$ and shows multiple resonant frequencies at 1.14, 1.91, and 2.45 GHz. Omnidirectional radiation patterns in the azimuth plane and vertical polarization at all operating frequency bands were obtained. Antenna gains greater than 1.7 dBi were obtained at the three operating frequencies, and the antenna height is 6 mm. Therefore, the proposed antenna is applicable to the vehicular telecommunication system.

1. INTRODUCTION

In vehicular telecommunication, low-profile multiband antennas are required due to ease installation, aerodynamics, and multiple operations, such as navigation, integrated mobile applications, automatic driving, and mayday services [1]. Moreover, vertical polarization and omnidirectional radiation characteristics are desired. This is because vertically polarized waves experience less propagation path loss compared to horizontally polarized waves, in the case of near-ground wireless communication [2], and the omnidirectional radiation in the azimuth plane covers the wide range of communication space.

Various antenna design approaches have been exploited to meet the aforementioned characteristics, i.e., low-profile, multiband operation, vertical polarization, and omnidirectional radiation [3–10]. For an effort, a lossy ferrite was inserted between a patch radiator and ground plane to reduce the antenna height to $0.005\lambda_L$, where λ_L is the wavelength at the lowest operating frequency of 30 MHz [3]. However, gain of the antenna was unreasonably low due to high magnetic loss of the ferrite. Another approach is to use fractal-based techniques to reduce antenna height, while maintaining a high antenna gain. The height of fractal monopole antenna was $0.153\lambda_L$ [4] or $0.34\lambda_L$ [5]. This height is still too high to apply to mobile vehicular applications. Lastly, a wire-patch antenna, comprised of a top patch and shorting pins, was introduced [6–10]. The wire-patch broadband antenna shows a high antenna gain with the height of $0.079\lambda_L$ [7], $0.078\lambda_L$ [8], or $0.07\lambda_L$ [9]. However, the antenna height is still not suitable for vehicle telecommunication systems. A $0.062\lambda_L$ high wire-patch antenna shows an omnidirectional radiation pattern with vertical polarization, but operates at a single frequency [10].

In this letter, we report design and performance of an omnidirectional low-profile multiband antenna for vehicular wireless communication applications. The designed antenna shows the height of $0.022\lambda_L$ with patch size of $0.26\lambda_L \times 0.3\lambda_L$ and omnidirectional radiation with vertical polarization at three operating frequency bands.

Received 9 December 2014, Accepted 3 January 2015, Scheduled 15 January 2015

* Corresponding author: Yang-Ki Hong (ykhong@eng.ua.edu).

[1] Department of Electrical and Computer Engineering, The University of Alabama, Tuscaloosa, Alabama 35487, USA. [2] E.M.W. Co., Ltd., Seoul 153-803, Republic of Korea.

2. ANTENNA DESIGN AND FABRICATION

Figure 1 shows the designed antenna structure and geometry, and the antenna has a rectangular patch (70 mm × 80 mm) and six shorting pins (diameter of 0.4 mm and height of 6 mm). The rectangular patch is divided into three sub-patches (sub-patches 1, 2, and 3) by slots 1 and 2 having 1.8 mm wide gap (g). These sub-patches are connected to one another by four connecting lines as shown in Figure 1. The length and width of the connecting lines are 1.8 mm and 1 mm, respectively. The six shorting pins are used to connect the sub-patches to a ground plane (200 mm × 200 mm). As shown in Figure 1(b), the two outermost shorting pins, named as the pin 1 in Figure 1(a), are symmetrically located from the center of the antenna and connect the sub-patch 1 to the ground plane. Likewise, the pin 2 (or pin 3) is used to connect the sub-patch 2 (sub-patch 3) to the ground. The antenna was then excited by a coaxial probe to characterize antenna performance. The coaxial probe is located at a 15.25 mm offset (in x-axis) from the center of the antenna and connected to the sub-patch 3. This feeding location was chosen because the gain increased from 1.3, 3.0, and 2.6 dBi to 1.7, 3.2, and 3.4 dBi at the first (f_1), second (f_2), and third resonant frequency (f_3), respectively, as the probe position moved from the center to an offset of 15.25 mm (in x-axis).

Antenna performance characteristics were simulated by three-dimensional (3D) electromagnetic simulation tool (ANSYS HFSS v. 11) for scattering parameters (S-parameters), surface current distribution, and radiation patterns. Based on the design geometry in Figure 1, an antenna was fabricated (not shown here). Copper plates and wires were used in the fabrication of the antenna radiator, ground plane, and shorting pins. The antenna has a total area of 5,600 mm^2 (70 mm × 80 mm) and height of 6 mm. The ground plane (200 mm × 200 mm) was used to take into account a vehicle roof. A semi-rigid 50 Ohm coaxial cable was used to excite the antenna. A vector network analyzer (Agilent N5230) and an anechoic chamber (Raymond EMC QuietBox AVS 700) were used to measure antenna S-parameters and radiation patterns.

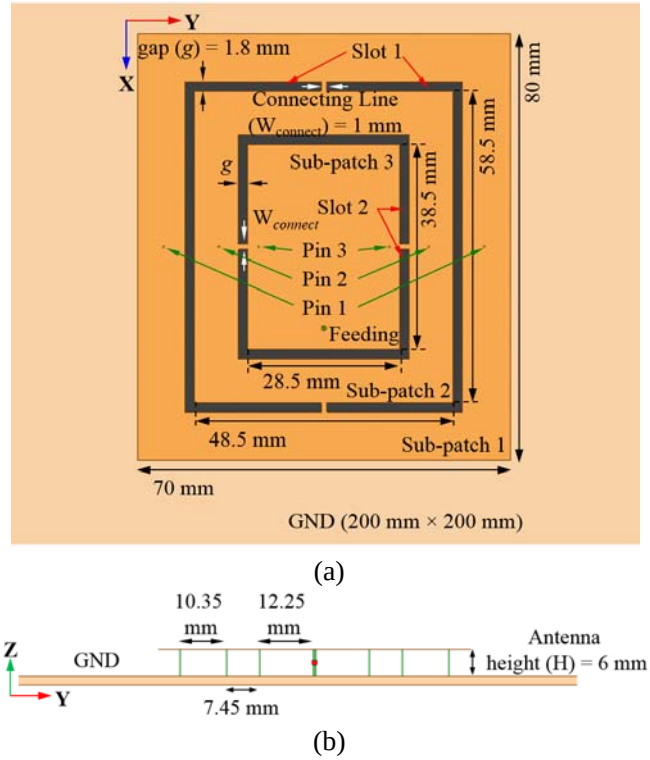

Figure 1. Design and geometry of an omnidirectional low-profile multiband antenna: (a) top view and (b) side view.

3. ANTENNA SIMULATION AND OPERATING PRINCIPLES

In order to study the operation principles of the proposed antenna, the effect of the slots on S-parameters is presented in Figure 2(a). No slot, slot 1, and slots 1 and 2 were independently loaded onto the rectangular patch, while all six shorting pins (pins 1, 2, and 3) exist. The 70 mm × 80 mm rectangular patch (without slots) with six shorting pins generates two resonant frequencies and different radiation characteristics. At the first resonant frequency (f_{1_s0}), the antenna showed an omnidirectional radiation pattern with vertical polarization in the azimuth plane (XY-plane). On the other hand, non-omnidirectional radiation pattern with horizontal polarization was observed at the second frequency (f_{2_s0}). The first resonance is a parallel resonant mode, originating from the inductance of the shorting pins set in parallel with the capacitance of the antenna [11]. The second is a top-loaded (quarter-wavelength) monopole resonant mode resulting from the capacitance from the top-loaded patch [7]. It was found that the antenna produces a strong vertically polarized electric field from the shorting pins at the parallel resonant mode, but a horizontally polarized electric field from the patch at the top-loaded resonant mode. By implementing slot 1, the parallel resonant mode is generated at two frequencies, f_{1_S1} and f_{3_S1}, while the top-loaded monopole resonant mode occurs at f_{2_S1} and f_{4_S1}. By adding slots 1 and 2 to the rectangular patch, three resonant frequencies with the parallel resonant mode were obtained. As a result, the omnidirectional radiation patterns in the azimuth plane with vertical polarization were observed at f_1, f_2, and f_3. The first-resonant reflection coefficients at f_{1_S0} (1.26 GHz: no slot), f_{1_S1} (1.18 GHz: slot 1), and f_1 (1.09 GHz: slots 1 and 2) were −16.6 dB, −16.5 dB, and −6.2 dB, respectively. The inserting slots caused a decrease in the input impedance at the first resonant mode, resulting in an impedance mismatch. In addition, slots 1 and 2 lead to frequency shift towards lower frequency due to the additional series inductance.

Figure 2(b) shows the effect of the shorting pins on S-parameters of the antenna while maintaining slots 1 and 2. The result of shorting pins 1, 2, and 3 in Figure 2(b) corresponds to the data of slots 1 and 2 in Figure 2(a). When only pin 1 was added, the parallel resonant mode was observed at frequencies f_{1_P1} and f_{2_P1}. By inserting all three pins (1, 2, and 3), the antenna showed the parallel resonant mode at three frequency bands and improved impedance matching at f_2 and f_3 as shown in Figure 2(b). However, the first-resonant reflection coefficient increased from −17.3 dB (f_{1_P2} = 1.07 GHz: pin 1 and 2) to −6.2 dB (f_1 = 1.09 GHz: pin 1, 2, and 3). This is because an addition of pin 3 introduces a parallel inductance and results in a decrease in the first-resonant input impedance. It is noted that the double resonance was observed near the third resonant mode (i.e., f_3 and $f_{3\text{-}2}$) as shown in Figure 2. The resonant frequency, $f_{3\text{-}2}$, is due to the self-resonance of the slots regardless of the shorting pins. The proposed antenna exhibits three resonant frequencies, f_1, f_2, and f_3, of 1.09, 1.86, and 2.39 GHz.

Figure 3 shows simulated vector surface current distributions at the three resonant frequencies

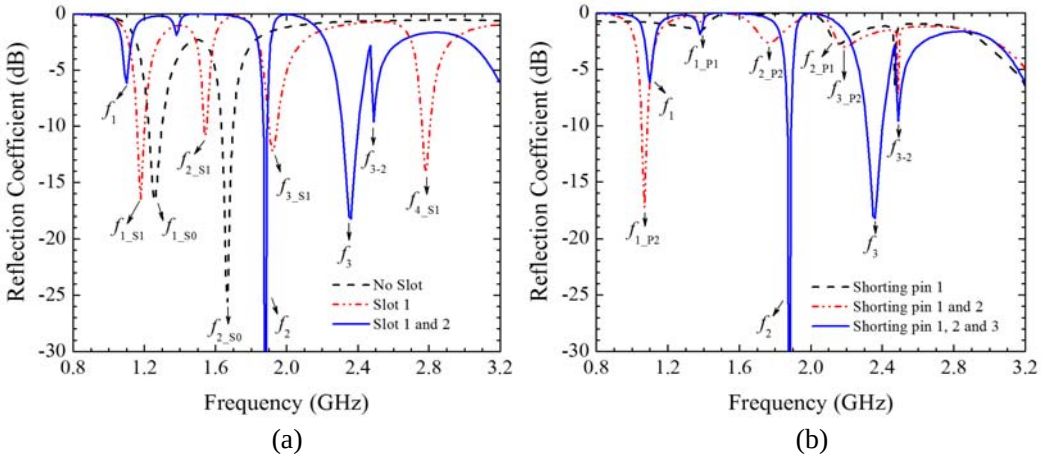

Figure 2. Simulated reflection coefficient of the proposed omnidirectional low-profile multiband antenna: (a) effect of slots and (b) effect of shorting pins.

that help to understand multiband operation with the parallel resonant mode. Current flows from the feeding line to the patches, then shorts to the ground via shorting pins at the resonant frequencies. This indicates that the parallel resonant mode occurs at each resonant frequency [7]. Moreover, the antenna has different current paths from the feeding line through the sub-patches and shorting pins at each resonant frequency. At the f_1, high current density appears in a current path from the feeding line through all three sub-patches (i.e., sub-patches 3, 2, and 1) and the outermost pin 1 as shown in Figure 3(a). At the f_2, the antenna has a current path from the feeding line through two sub-patches (i.e., sub-patches 3 and 2) and pin 2. The shortest current path from the feeding line through the sub-patch 3 and pin 3 occurs at the f_3. It is noted that strong surface current is concentrated at the

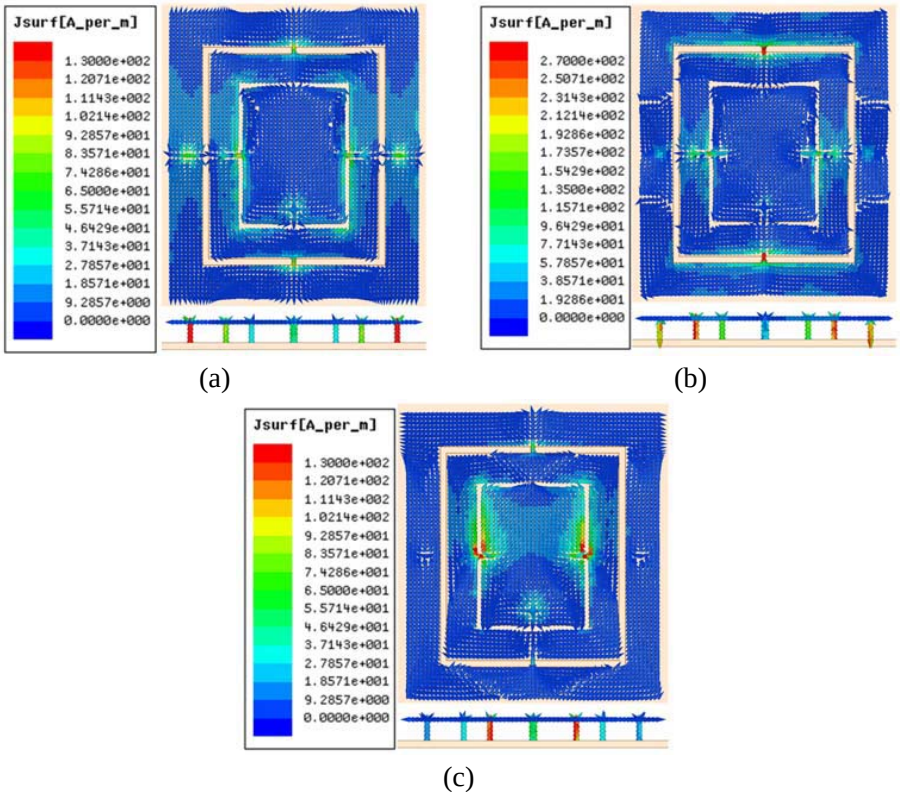

Figure 3. Simulated vector surface current distribution: at (a) f_1 of 1.09 GHz, (b) f_2 of 1.86 GHz, and (c) f_3 of 2.39 GHz.

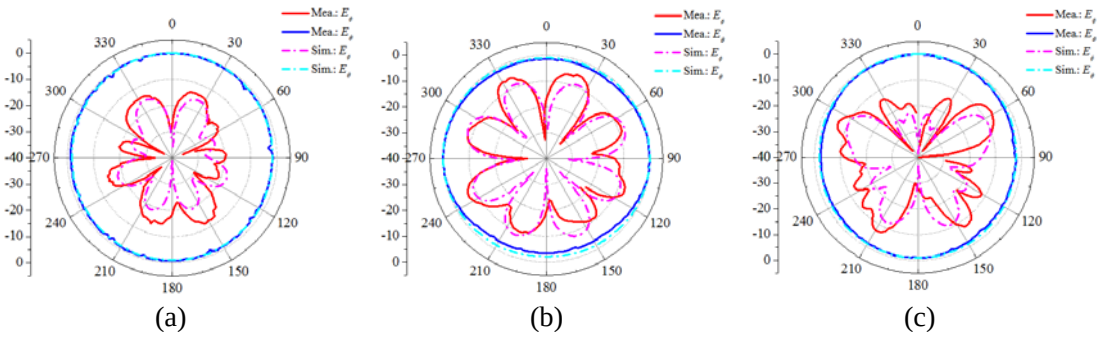

Figure 4. Simulated and measured radiation patterns in azimuth plane at (a) f_1 (sim.: 1.09 GHz and mea.: 1.14 GHz), (b) f_2 (sim.: 1.86 GHz and mea.: 1.91 GHz), and (c) f_3 (sim.: 2.39 GHz and mea.: 2.45 GHz), respectively.

vertically mounted shorting pins, while relatively weak current density appears at the horizontal sub-patches at the three resonant frequencies. The strong vertical current in the shorting pins, therefore, leads to omnidirectional radiation and vertical polarization in the azimuth plane.

Figure 4 shows the simulated radiation patterns in the azimuth plane. The antenna shows the omnidirectional radiation characteristics with vertical polarization at the three resonant frequencies. The simulated maximum ripple levels ($\Delta = E_{\theta\_\max} - E_{\theta\_\min}$) are 1.8 dB at f_1 (1.09 GHz), 2.1 dB at f_2 (1.86 GHz), and 2.1 dB at f_3 (2.39 GHz), thereby confirming omnidirectional radiation patterns. Furthermore, the vertical component E_θ of electric field is greater than the horizontal component E_ϕ of electric field as shown in Figure 4.

4. MEASURED RESULTS AND DISCUSSION

Figure 5 shows both measured and simulated S-parameters. Antenna resonates at 1.14, 1.91, and 2.45 GHz, which are in close agreement with the simulated results. Small discrepancy between the simulated and measured S-parameters is attributed to fabrication inaccuracy. The fabricated antenna has a low-profile of $0.022\lambda_L$ (where λ_L is the wavelength at f_1). The measured and simulated radiation patterns in the azimuth and elevation (XZ-plane) planes are shown in Figures 4 and 6. In Figure 4, the measured maximum ripple levels in the azimuth plane are 1.9 dB at the f_1 (1.14 GHz), 3.6 dB at the f_2 (1.91 GHz), and 2.5 dB at the f_3 (2.45 GHz). These results confirm omnidirectional radiation

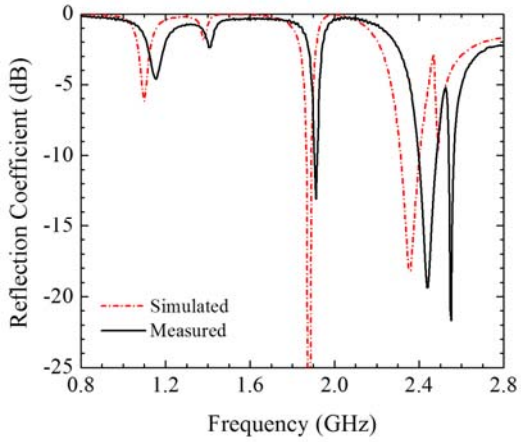

Figure 5. Simulated and measured S-parameters of the fabricated omnidirectional low-profile multiband antenna.

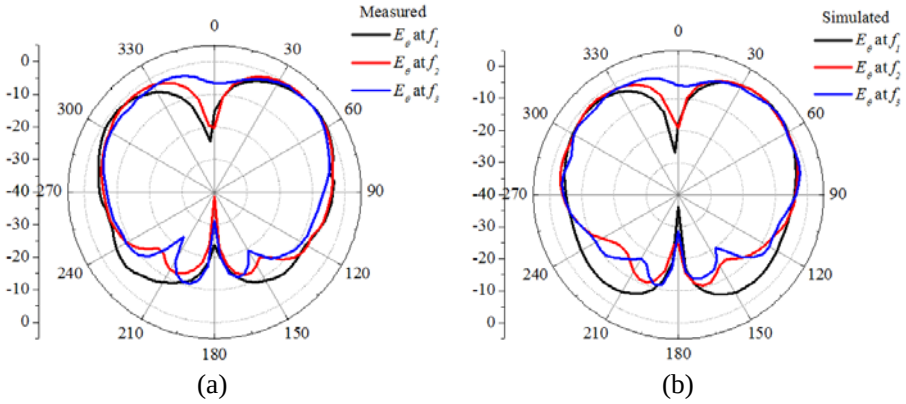

Figure 6. Radiation patterns of E_θ in elevation plane at each resonant frequency: (a) measured and (b) simulated radiation pattern.

Table 1. Simulated and measured characteristics of the proposed antenna.

	f_1		f_2		f_3	
	Sim.	Mea.	Sim.	Mea.	Sim.	Mea.
Resonant freq. (GHz)	1.09	1.14	1.86	1.91	2.39	2.45
Electrical height (6 mm)	0.021λ	0.022λ	0.037λ	0.038λ	0.047λ	0.049λ
Max. ripple (dB)	1.8	1.9	2.1	3.6	2.1	2.5
Polarization	Vertical	Vertical	Vertical	Vertical	Vertical	Vertical
3D peak gain (dBi)	1.7	1.7	3.2	4	3.4	3.5

Table 2. Comparison of antenna characteristics for omnidirectional low-profile antennas.

	Antenna height at f_L	Antenna patch size at f_L	Gain (dBi)	Ripple level (dB)	Band
Ref. [7]	$0.079\lambda_L$	D (diameter): $0.5\lambda_L$	> 3	< 1.7	Wideband
Ref. [8]	$0.078\lambda_L$	D: $0.31\lambda_L$	> 2.3	< 1.8	Wideband
Ref. [9]	$0.07\lambda_L$	D: $0.4\lambda_L$	-	< 7.9	Wideband
Ref. [10]	$0.062\lambda_L$	$0.27\lambda_L \times 0.33\lambda_L$	4.5	-	Single-band
This work	$0.022\lambda_L$	$0.26\lambda_L \times 0.3\lambda_L$	> 1.7	< 3.6	Multi-band

characteristics. In addition, the measured patterns are in good agreement with the simulated results. It is noted that the vertical component of E_θ is greater than the horizontal component E_ϕ, indicating the vertically polarized waves. The antenna also shows monopole-like radiation patterns in the elevation plane as shown in Figure 6. The maximum measured gain was found near $\theta = \pm 40^\circ$. The measured 3D peak gain is 1.7 dBi (at $\theta = 50^\circ$) at the f_1, 4 dBi (at $\theta = 40^\circ$) at the f_2, and 3.5 dBi (at $\theta = 40^\circ$) at the f_3, which are in good agreement with the simulated gains (1.7 dBi at the f_1, 3.2 dBi at the f_2, and 3.4 dBi at the f_3). The measured and simulated characteristics are summarized in Table 1. It is demonstrated that the proposed antenna has a low-profile, omnidirectional radiation, and vertical polarization at the three frequency bands. For comparison, the antenna characteristics of the proposed and previously reported omnidirectional low-profile antennas are given in Table 2. The proposed antenna shows a considerably small height with multiband operation, while retaining good antenna gains and low ripple levels. Although the proposed antenna shows good far-field radiation characteristics, impedance matching and bandwidth at the f_1 needs to be improved. Enhancements in impedance matching and bandwidth are under investigation by magneto-dielectric material loading [12] and capacitive loading techniques [13].

5. CONCLUSION

A low-profile vertically-polarized omnidirectional multiband antenna is proposed. The measured antenna performance is in good agreement with the simulated results. The antenna is only $0.022\lambda_L$ in the height and has a patch size of $0.26\lambda_L \times 0.3\lambda_L$ with multiple resonant frequencies of 1.14, 1.91, and 2.45 GHz. Furthermore, the antenna shows good omnidirectional radiation characteristics with vertical polarization and high antenna gain. Therefore, the low-profile multiband antenna is applicable to vehicular telecommunications.

REFERENCES

1. Leelaratne, R. and R. Langley, "Multiband PIFA vehicle telematics antennas," *IEEE Trans. Veh. Technol.*, Vol. 54, 477–485, 2005.
2. Liao, D. and K. Sarabandi, "Terminal-to-terminal hybrid full-wave simulation of low-profile, electrically small, near-ground antennas," *IEEE Trans. Antennas Propag.*, Vol. 56, 806–814, 2008.

3. Moon, H., G.-Y. Lee, C.-C. Chen, and J. L. Volakis, "An extremely low-profile ferrite-loaded wideband VHF antenna design," *IEEE Antenn. Wireless Propag. Lett.*, Vol. 11, 322–325, 2012.
4. Puente-Baliarda, C., J. Romeu, R. Pous, and A. Cardama, "On the behavior of the Sierpinski multiband fractal antenna," *IEEE Trans. Antennas Propag.*, Vol. 46, 517–528, 1998.
5. Puente-Baliarda, C., J. Romeu, and A. Cardama, "The Koch monopole: A small fractal antenna," *IEEE Trans. Antennas Propag.*, Vol. 48, 1773–1781, 2000.
6. Delaveaud, C., P. Leveque, and B. Jecko, "New kind of microstrip antenna: The monopolar wire-patch antenna," *Electron. Lett.*, Vol. 30, 1–2, 1994.
7. Lau, K.-L., P. Li, and K.-M. Luk, "A monopolar patch antenna with very wide impedance bandwidth," *IEEE Trans. Antennas Propag.*, Vol. 53, 1004–1010, 2005.
8. Lau, K.-L. and K. M. Luk, "A wide-band monopolar wire-patch antenna for indoor base station applications," *IEEE Antenn. Wireless Propag. Lett.*, Vol. 4, 155–157, 2005.
9. Zheng, S.-F., Y.-Z. Yin, X.-S. Ren, Z.-Y. Liu, and L. Kang, "A wide band low-profile monopolar patch antenna," *Microw. Opt. Technol. Lett.*, Vol. 53, 28–32, 2011.
10. Baek, S. and S. Lim, "Low-profile planar roof-mounted vehicle antenna for monopole vertical polarization reception," *Microw. Opt. Technol. Lett.*, Vol. 54, 91–94, 2012.
11. Seaus, J. P., A. Reineix, and B. Jecko, "Susceptibilite aux impulsions electromagnetiques parasites des antennas plaquees sur substrat dielectrique," *Annales des Telecommunications*, Vol. 45, 3–4, 1990.
12. Lee, J., Y.-K. Hong, W. Lee, G. S. Abo, J. Park, W.-M. Seong, and S. Bae, "Role of small permeability in gigahertz ferrite antenna performance," *IEEE Magn. Lett.*, Vol. 4, 5000104, 2013.
13. Oh, J. and K. Sarabandi, "Low profile vertically polarized omnidirectional wideband antenna with capacitive parasitic elements," *IEEE Trans. Antennas Propag.*, Vol. 62, 977–982, 2014.